Leakage Performance and Breakdown Mechanism of Silicon-Rich Oxide and Fluorinated Oxide Prepared by Electron Cyclotron Resonance Chemical Vapor Deposition

Kow Ming Chang, Shih Wei Wang, Ta Hsun Yeh, Chii Horng Li, and Jiunn Jye Luo

Department of Electronic Engineering and Institute of Electronics, National Chiao Tung University, National Nano Device Laboratory, Hsinchu, Taiwan

ABSTRACT

The characteristics of silicon-rich oxide and fluorinated oxide (F_xSiO_y) films deposited in an electron cyclotron resonance chemical vapor deposition system with SiH_4 and O_2 as the oxide sources and CF_4 as the fluorinating precursor are investigated in this work. According to experimental results, the dangling bonds in Si-rich oxide behave as positively by charged electron traps and degrade the dielectric strength by lowering the barrier height for Fowler-Nordheim tunneling. On the other hand, a small amount of incorporated F atoms will passivate and neutralize these excess Si dangling bonds, thereby elevating the dielectric strength. However, too much incorporated F will degrade the pretunneling leakage performance owing to the porosity and fatigues structure in F_xSiO_y film. The high leakage and even breakdown at low field strongly limits the incorporated F concentration in F_xSiO_y film and the lowering of dielectric constant.

Introduction

Advances in ultralarge-scale integrated circuits have led to the necessity for an intermetal dielectric (IMD) with the dielectric constant (k) as low as possible to overcome the limitation of signal delay. As a candidate for low-k IMD material, chemical vapor deposition of inorganic fluorinated silicon oxide (F_xSiO_y) has received extensive interest due to its easily integratable properties and various readily available precursors.[1-13] In addition to low dielectric constant, maintaining the other properties desirable for IMD applications (such as low leakage current, low mechanical stress, high thermal stability, and low moisture absorption) is also important. However, only a few studies have been published on these issues,[11,13] especially for those dedicated to the leakage performance and dielectric strength of F_xSiO_y. On the other hand, Si-rich oxide (SiO_y, $y \leq 2$) prepared by electron cyclotron resonance chemical vapor deposition (ECR-CVD), capable of preventing moisture permeation and avoiding hot carrier effects, is very important to back-end applications.[12,14-17] Similarly, there has been very little work on the leakage performance and dielectric strength of ECR-SiO_y.

In this work, ECR-CVD Si-rich SiO_y and F_xSiO_y films for IMD applications were fabricated, with SiH_4 and O_2 as the oxide sources and CF_4 as the fluorinating precursor. According to experimental results, the change in stoichiometry, controlled by the flow ratio of SiH_4/O_2, heavily affects the dielectric constant and electrical performance of Si-rich SiO_y. The excess Si dangling bonds, acting as positively charged electron traps, are shown to degrade the dielectric strength of the oxide. On the other hand, not only reducing the dielectric constant, the small amount of incorporated F atoms will passivate and neutralize these excess Si dangling bonds and be of benefit to the dielectric strength of the deposited film. However, too much incorporated F leads to a porous and fatigued oxide network. The pretunneling leakage performance of F_xSiO_y is found to degrade with the increase of F concentration and even break down at a low field. Such an event strongly affects the reliability and applicability of F_xSiO_y. The mechanisms contributing to these results are discussed in this paper.

Experimental

Figure 1 shows the schematic diagram of the ECR system used in this work. High-density plasma of O_2/CF_4 was ignited by microwave (MW) with a frequency of 2.45 GHz and magnetic field at 875 G. The O_2/CF_4 plasmas downstream and react with SiH_4 injected from the gas ring. The SiO_y and F_xSiO_y films were deposited on 4 in., (100)-oriented, p-type silicon wafers. The wafers were treated with RCA cleaning and dipped in HF solution (1/100) before loading. The O_2 flow rates were fixed at 85 sccm while the SiH_4 flow rates were varied from 2 to 10 sccm, and the CF_4 flow rates were varied from 0 to 20 sccm. The deposition pressure was kept at 3 mTorr. The deposition temperature (T) was varied from 25 to 300°C and MW power was set at 250 or 300 W.

The composition and chemical bonding structure of deposited films were investigated by x-ray photoelectron spectroscopy (XPS) and Fourier transform infrared spectroscopy (FTIR), respectively. The dielectric constants (k) were measured from C-V characteristics using a Keithley C-V system with a simple metal-insulator-semiconductor (MIS) structure at 1 MHz. The refractive index and thickness of the deposited films were determined by ellipsometry at a frequency of 632.8 nm (He-Ne laser). The I-V characteristics and variation of voltage drop on the deposited film, under constant current stress, were investigated by using an HP4145B system with MIS structure.

Results and Discussion

Figure 2 depicts the typical XPS spectra of ECR-SiO_y (CF_4 = 0 sccm) and F_xSiO_y films. Four main elements: Si (2s, 2p), C (1s), O (1s), and F (1s), are observed in the deposited films. The incorporated F concentration (1s, 687 eV) increases with the increased CF_4 flow rate. The high flow ratio of O_2 to CF_4 effectively limits the concentration of incorporated C to less than 2 atomic percent (a/o) due to

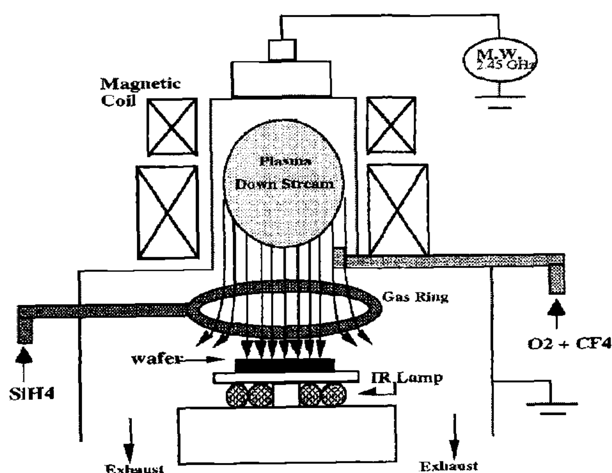

Fig. 1. Schematic diagram of ECR-CVD system.

Downloaded on 2014-04-28 to IP 140.113.38.11 address. Redistribution subject to ECS terms of use (see ecsdl.org/site/terms_use) unless CC License in place (see abstract).

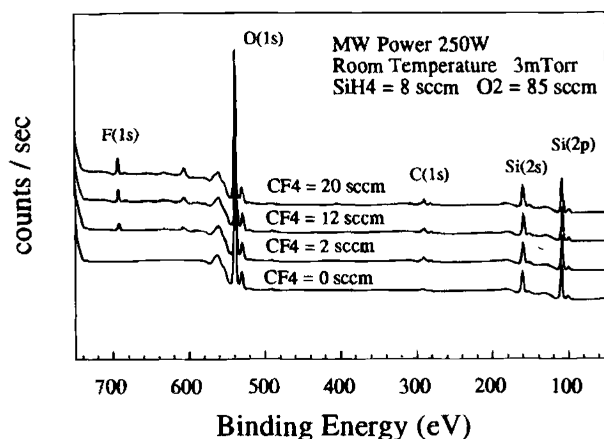

Fig. 2. Typical XPS spectra of the F_xSiO_y film with different CF_4 flow rates.

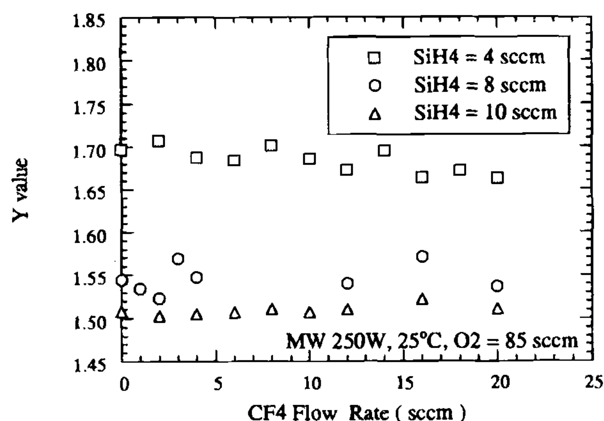

(a)

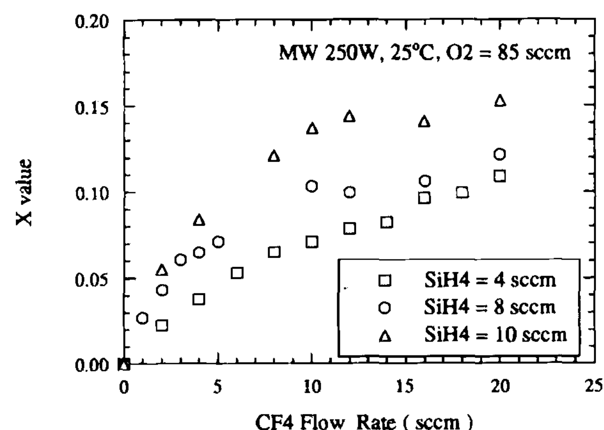

Fig. 3. Variations of (a) y value and (b) x value in stoichiometry of F_xSiO_y films, with different SiH_4, CF_4 flow rates.

the oxidation effect. Quantitative measurement from XPS spectra also demonstrates that ECR-SiO_y is nonstoichiometric and Si-rich in composition. From Fig. 3a, a higher flow ratio of SiH_4 over O_2 results in a richer Si in oxide composition. From FTIR spectra, such stoichiometric change of oxide with SiH_4/O_2 flow ratio is reflected in the variation of Si-O-Si stretching vibration frequency, as shown in Table I. The stretching vibration frequency of thermal oxide (1000°C, O_2 dry oxidation) is about 1087.7 cm^{-1}. On the other hand, for ECR-SiO_y films deposited at 300°C, the vibration frequency shifts from 1074.4 cm^{-1} for SiH_4/O_2 = 2/85 sccm, to 1057.6 cm^{-1} for SiH_4/O_2 = 10/85 sccm. According to the work of Kobeda *et al.*,[18] the stretching vibration frequency (ν) of Si-O-Si in glass network depends on its common angle [θ, where $\nu \propto \sin(\theta/2)$]. Additionally, the Si-rich oxide tends to have a smaller θ according to the structure-induced charge-transfer model (SICT).[19] Therefore, the decrease of Si-O stretching vibration frequency accounts for the richer Si in oxide composition. The richer Si in ECR-SiO_y oxide results in a higher dielectric constant (k) than that of stoichiometric thermal oxide, as shown in Table I. This is due to the excess Si (dangling bonds) which results in the strain and disturbs the balance position of other atoms in ideal oxide and induces an excess dipole moment.

Not only the stoichiometric ratio of Si over O, the SiH_4/O_2 flow ratio also affects the incorporated F concentration in F_xSiO_y when CF_4 is added. The stoichiometry y value of F_xSiO_y film almost keeps constant, while the x value monotonically increases with an increasing CF_4 flow rate (0 to 20 sccm), as shown in Fig. 3a and b, respectively. This result demonstrates that with both behaving as the electron acceptors, there is no competition between active F and O species if there is enough Si source for a reaction. The incorporated F atoms passivate and reduce the Si dangling bond concentration with the formation of Si-F bonds, as shown in Fig. 4. Moreover, the ECR-F_xSiO_y with richer Si in composition (*i.e.*, higher SiH_4/O_2 ratio) will involve more incorporated F. In Fig. 3a and b, the incorporated F concentration rises from 3.9 a/o for SiH_4/O_2 = 4/85, 4.6 a/o for SiH_4/O_2 = 8/85, toward 5.9 a/o for SiH_4/O_2 = 10/85 sccm, with the same CF_4 (20 sccm) added. The dielectric constant of F_xSiO_y film also decreases from 3.13 for $SiH_4/O_2/CF_4$ = 8/85/20 sccm to 2.98 for $SiH_4/O_2/CF_4$ = 10/85/20 sccm, correspondingly.

According to the work of Takahashi *et al.*,[14] the dangling bonds belonging to Si atoms in ECR oxide are amorphous centers ($Si_3 \equiv Si-$) and E′ centers ($O_3 \equiv Si-$) or oxygen vacancies. The water-blocking ability comes from these defect centers and hydrogen-passivated Si bonds (Si-H).[14-17] The hot carrier degradation was shown to be reduced with increasing the SiH_4/O_2 flow ratio during deposition of the ECR-SiO_y water blocking layer.[17] Unfortunately, according to our experimental results, the dielectric strength of ECR-SiO_y heavily degrades with an increasing SiH_4/O_2 flow ratio. Figure 5 shows the time-zero dielectric breakdown characteristics of thermal oxide (1000°C, O_2 dry oxidation) and ECR-SiO_y films (300°C, with various SiH_4/O_2 flow ratios) taken at room temperature. The thickness of

Table I. Changes in FTIR Si-O stretching vibration frequency, dielectric constant (1 MHz), and barrier height for Fowler-Nordhein tunneling[20] at an Al-insulator interface for thermal oxide (dry oxidation) and ECR-CVD oxides (300°C, MW 300 W, 85 sccm O_2) deposited with various SiH_4 flow rates.

Insulator type (~100 nm)	FTIR Si-O stretching peak (cm^{-1})	Dielectric constant	F-N barrier height (eV)
Thermal oxide (O_2, 1000°C)	1087.7	3.98	3.304
ECR oxide, 2 sccm SiH_4	1074.4	4.22	2.316
ECR oxide, 4 sccm SiH_4	1066.6	4.39	2.259
ECR oxide, 8 sccm SiH_4	1059.3	4.51	2.248
ECR oxide, 10 sccm SiH_4	1057.6	4.57	0.533

Downloaded on 2014-04-28 to IP 140.113.38.11 address. Redistribution subject to ECS terms of use (see ecsdl.org/site/terms_use) unless CC License in place (see abstract).

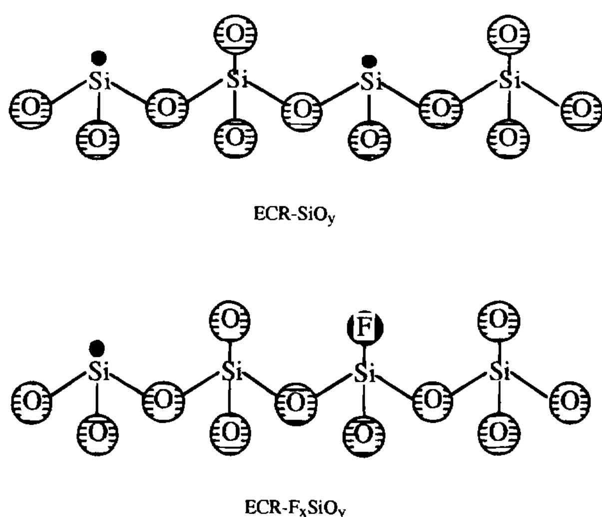

Fig. 4. Hypothesized local structures in Si-rich ECR-SiO_y and F_xSiO_y film networks. Part of Si dangling bonds (●) are passivated with F bonds with the addition of CF_4.

all dielectrics is around 100 nm. Polarity of the field causes carrier accumulation at the Si surface corresponding to electron injection from the metal gate. The breakdown field degrades rapidly with the increasing SiH_4/O_2 flow ratio, in comparison to that of near-stoichiometric thermal oxide. From the current density (J) *vs.* electric field (E) curves, the linearity for the ln (J/E^2) *vs.* 1/E relationship demonstrates that the barrier for Fowler-Nordhein tunneling[20] generally decreases with increasing the SiH_4/O_2 flow ratio, as shown in Table I. The measured slope, corresponding to barrier height at the aluminum/oxide interface, drops from 3.304 eV for thermal oxide toward 0.533 eV for ECR-SiO_y with SiH_4/O_2 = 10/85 sccm. According to Maserjian and Zamani,[21] Balland,[22] and Hasegawa *et al.*,[23] the oxygen vacancies induce positive fixed charges in the oxide. Figure 6 compares the high-frequency C-V curves for well-controlled thermal oxide and Si-rich ECR-SiO_y. The negative shifting of flatband voltage (V_{FB}) accounts for the existence of positive charges in ECR-SiO_y. As a result, the barrier lowering is assumed to be due to the image force effect of positive oxide charges acting on the metal/oxide interface.[24] In addition, the local potential well of positive charged centers also contributes to the tunneling current.[25] For a thick oxide, the injected elec-

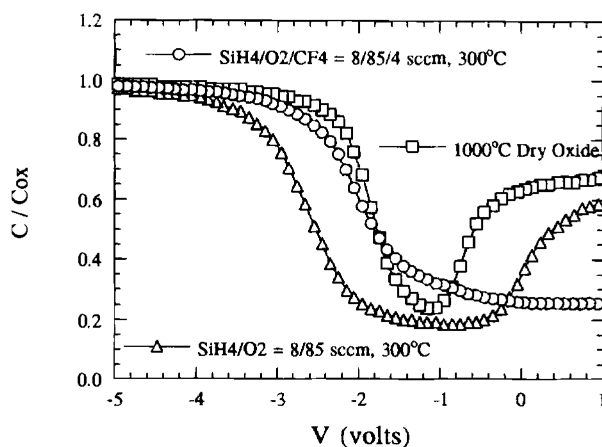

Fig. 6. High-frequency C-V characteristics of thermal oxide, ECR-SiO_y and F_xSiO_y (MW 300 W, 3 mTorr and 300°C), with thickness around 100 nm.

trons result in impact ionization near the anode (>9 eV)[26] due to the large voltage drop on the oxide even under a low electric field. Therefore, dielectric strength rapidly degrades with an increasing SiH_4/O_2 flow ratio.

Concurrently, a large amount of defect centers (E′ center and Si-H bonds) in Si-rich oxide is also responsible for dielectric breakdown.[23] Researchers on E′ centers have suggested that they act as hole traps,[27] some electron traps,[28] and still others that they are both electron traps and hole traps.[29-33] In the present work, the trapping centers in ECR-SiO_y are shown to be electron traps and increase in amount with the SiH_4/O_2 flow ratio. Figure 7 reveals the changes of voltage drop on the oxide ($\Delta|V_g-V_{FB}|$) under constant current stress in the range of F-N tunneling. The increase of voltage drop, required to maintain a constant current, reflects the existence of electron trapping centers in oxide.[34] It is found that the voltage drop on thermal oxide almost keeps constant without change, while the voltage drop on ECR-SiO_y increases during stress. On the other hand, the change of voltage drop on ECR-SiO_y also increases with increasing the SiH_4/O_2 flow ratio under the same charge fluence. As a result, the richer the Si in oxide composition, more trapping centers are present. The Si dangling bonds may be passivated with –H bonds in more humid air. However, the Si-H bonds are easily broken by energetic electrons (>2 eV)[26] and become E′

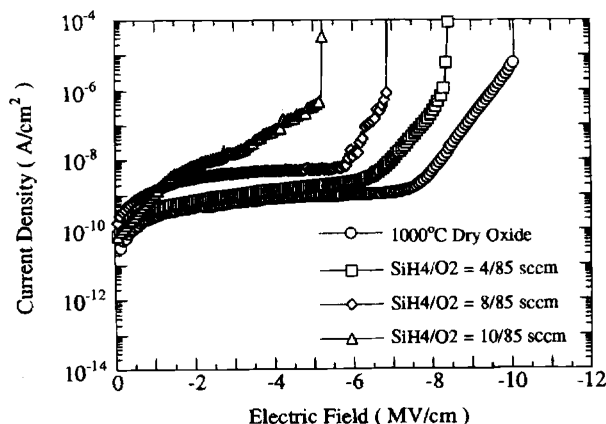

Fig. 5. Time-zero dielectric breakdown characteristics of the thermal oxide (dry oxidation, 1000°C) and the ECR-SiO_y films (MW 300 W, 3 mTorr, and 300°C) deposited with different SiH_4/O_2 flow ratios.

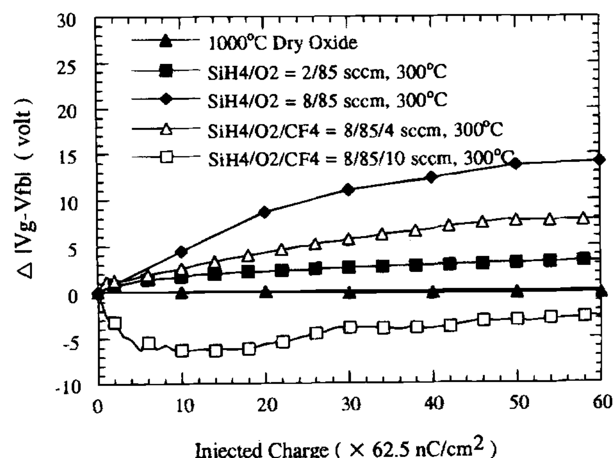

Fig. 7. The changes of voltage drop ($\Delta|V_g - V_{FB}|$) on various oxide films during the constant current stress. The stress current was 0.1 nA with density ~62.5 nA/cm², in the range of F-N tunneling.

Downloaded on 2014-04-28 to IP 140.113.38.11 address. Redistribution subject to ECS terms of use (see ecsdl.org/site/terms_use) unless CC License in place (see abstract).

centers again. This result supports the conclusion in Hasegawa *et al.*'s work.[23] From literature reviews,[35-39] electron traps contribute to dielectric breakdown because the trapping of injected electrons will modulate the conduction band of the oxide and increase the positive feedback current.

On the other hand, it was found that the dielectric was strengthened with suitable incorporation of F. Figure 8 compares the time-zero dielectric breakdown characteristics of the ECR-SiO_y and F_xSiO_y films deposited at 300°C. The destructive breakdown fields of ECR-SiO_y films (with SiH_4/O_2 = 8/85 and 10/85 sccm) were enhanced with a little CF_4 added (4 sccm). From previous discussion and the comparison between C-V curves of ECR SiO_y and F_xSiO_y in Fig. 6, the incorporated F atoms passivate and neutralize the positive charged Si dangling bonds with the formation of Si–F bonds. The decrease of positive charges in the oxide accounts for the positive shifting of the C-V curve with the addition of CF_4. Therefore, the image force effect on barrier lowering, due to the positive oxide charge, is suppressed and responsible for the enhancement of breakdown field. From Fig. 8, the barrier height for F-N tunneling at the aluminum/oxide interface increases from 2.248 eV of ECR-SiO_y (SiH_4/O_2 = 8/85 sccm) to 2.288 eV of F_xSiO_y ($SiH_4/O_2/CF_4$ = 8/85/4 sccm), correspondingly. The Si–F bond has been shown to have higher strength (~5.73 eV) than that of the Si–H bond (~5.45 eV) to resist energetic electrons.[40] Such a decrease in electron trap concentration with the addition of CF_4 will be reflected in the change of voltage drop on the oxide during constant current stress. As shown in Fig. 7, the change of voltage drop during stress on F_xSiO_y, with $SiH_4/O_2/CF_4$ = 8/85/4 sccm, is suppressed compared to that on ECR-SiO_y without adding CF_4.

However, the pretunneling leakage performances of F_xSiO_y were found to degrade with further increasing the CF_4 flow rate. As shown in Fig. 8, the pretunneling leakage current of F_xSiO_y, with a higher amount of incorporated F ($SiH_4/O_2/CF_4$ = 10/85/12 sccm) ramps-up rapidly with field and even wears out a low field. Such a degradation of pretunneling leakage performance heavily impacts the applicability of F_xSiO_y within the normal operation range of IMD. According to experimental results, the high leakage current strongly correlates to the porous, fatigued structural network of F_xSiO_y. From prior reports,[12,13] the incorporation of F results in a porous oxide network due to its high electronegativity in nature and nonbridging termination with Si atoms. The porosity of the oxide can be determined from the changes in refractive index,[12] moisture permeation,[12] deposition rate,[13] and mechanical stress during the thermal cycle, with the addition of CF_4. Figure 9 depicts the variation of film stress during thermal cycling (25 to 400°C) with different F concentrations. The measured stress (σ_{total}) for the deposited film is the combination of intrinsic stress (σ_{int}) and thermal stress (σ_{th}).[41] The intrinsic stress is created when the film network is formed while the thermal stress is induced by the difference between the thermal expansion coefficient of the Si substrate (α_s) and that of the deposited film (α_f) when the film is cooled from the deposition temperature (T_{depo}) to room temperature (T_{RT})

$$\sigma_{total} = \sigma_{int} + \sigma_{th} \quad [1]$$

$$\sigma_{th} = \left[\frac{E}{1-\nu}\right](\alpha_s - \alpha_f)(T_{RT} - T_{depo}) \quad [2]$$

In Eq. 2, E and ν stand for Young's modules and Poisson's ratio of the deposited film, respectively. In Fig. 9, the higher thermal expansion coefficient of the Si substrate than that of the oxide in the elastic range contributes to the compressed stress of deposited films. The 300°C deposited F_xSiO_y film does not absorb moisture[12] and shows no hysteresis variation in stress during thermal cycles. This means no plastic deformation and structure change in the deposited film during the thermal cycle, and the stress at 300°C will be the intrinsic component. Therefore, the intrinsic (compressed) stresses are shown to relax with the addition of F. On the other hand, the stress variation with temperature in the elastic range is governed by the following equation

$$\frac{d\sigma_{total}}{dT} = \frac{d\sigma_{th}}{dT} = \left[\frac{E}{1-\nu}\right](\alpha_s - \alpha_f) \quad [3]$$

From Fig. 9, the $d\sigma_{th}/dT$ of the oxide decreases with the incorporation of F. This is due to the decrease of E or the increase of α_f. In F_xSiO_y films, the F atom forms a nonbridge terminal bond on one Si atom without linking to the other Si atoms. Additionally, the repulsive force between Si–F and Si–F bonds, or Si–F and Si–O bonds, further fatigues the oxide structure; thus, the resulting less rigid glass network and lower Young's modulus are reasonable.

Figure 10 reveals the general effect of incorporated F concentration on the pretunneling leakage performance of F_xSiO_y films about 250 nm thick. The leakage current density is about 1 nA/cm^2 at 1 MV/cm for ECR-SiO_y, and there is about an order of magnitude increase (~20 nA/cm^2) when 10 sccm of CF_4 is added. On the other hand, a lower

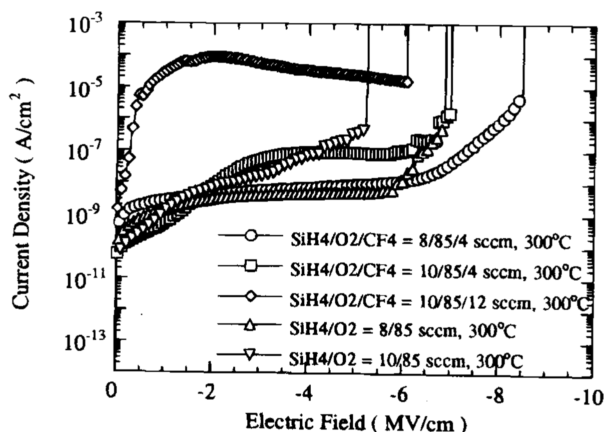

Fig. 8. Time-zero dielectric breakdown characteristics of ECR-SiO_y and F_xSiO_y films deposited with different $SiH_4/O_2/CF_4$ flow ratios (MW 300 W, 3 mTorr and 300°C).

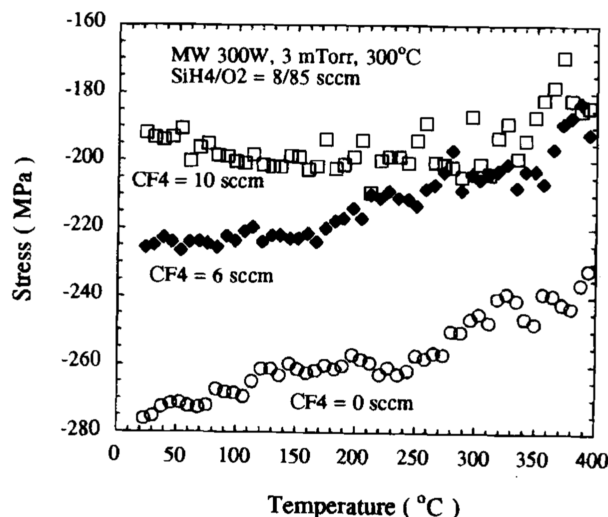

Fig. 9. Variation of mechanical stress during thermal cycles, from 25 to 400°C, for ECR-SiO_y and F_xSiO_y films deposited with different CF_4 flow rates.

Downloaded on 2014-04-28 to IP 140.113.38.11 address. Redistribution subject to ECS terms of use (see ecsdl.org/site/terms_use) unless CC License in place (see abstract).

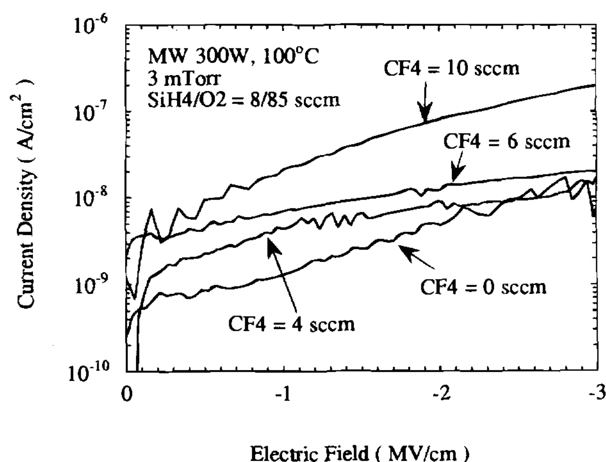

Fig. 10. Variation of F_xSiO_y film pretunneling leakage performance with different CF_4 flow rates.

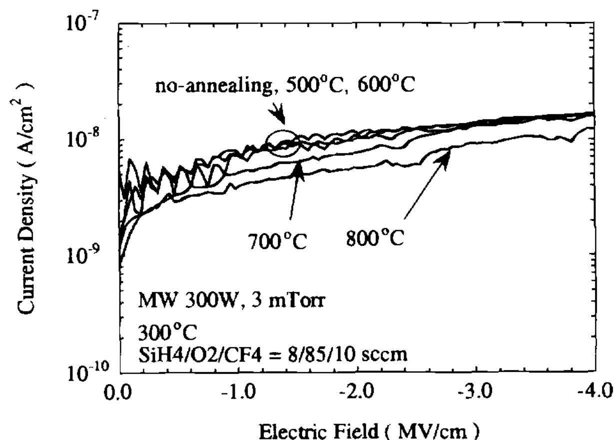

Fig. 12. Variation of pretunneling leakage performance for F_xSiO_y films, deposited at 300°C, before and after annealing at 500, 600, 700, and 800°C (30 min in N_2 ambient).

deposition temperature has been shown to result in a less dense stack and a higher, but unstable, incorporated F concentration in F_xSiO_y film.[12] Figure 11 depicts the general variation of pretunneling leakage current with electric field for the F_xSiO_y films deposited at various temperatures. The leakage performance generally degrades with decreasing deposition temperature. Besides, thermal stability of F also demonstrates the correlation between the F concentration and leakage performance. From prior work,[12] F_xSiO_y films deposited at 300°C were able to withstand annealing temperature above 700°C (N_2 ambient, 30 min) while the films deposited at 25°C could only withstand temperature about 500°C. Here we find that the leakage performance of F_xSiO_y films shows a similar tendency. Figure 12 depicts the pretunneling leakage of 300°C deposited film and those with subsequent annealing at 500, 600, 700, and 800°C (N_2 ambient, 30 min). Only slight changes were found at annealing temperatures above 700°C. On the other hand, the leakage performance of F_xSiO_y films deposited at 25°C shows profound changes after each temperature annealing, as shown in Fig. 13.

From this evidence, it can be seen that F incorporation indeed elevates the low-field leakage current in F_xSiO_y films. Although the Si dangling bonds can be passivated by F atoms, the porous structure and even micropores existing in the F_xSiO_y network additionally induces hole trap formation. Such an event can be realized by the decrease of voltage drop on F_xSiO_y, with $SiH_4/O_2/CF_4$ = 8/85/12 sccm, during the constant current stress, as shown in Fig. 7. According to Dumin and Muddux,[42] Rofan and Hu,[43] and Olivo *et al.*,[44] stress-induced traps and defects or weak spots in thin oxide are responsible for the excess low-level pretunneling current. In the present work, the fatigued structure and traps, contributing to a high pretunneling leakage current and catastrophic breakdown at low field through localized weak spots, are induced with the incorporation of F. Therefore, the power consumption and reliability problems which arise will limit the incorporated F concentration and hence the lowering of the dielectric constant of F_xSiO_y for IMD applications.

Conclusions

In summary, the stoichiometric change in Si-rich ECR-SiO_y relies on the flow ratio of SiH_4 over O_2. The Si dangling bonds (E′ centers or oxygen vacancies) behave as the electron traps with positive charged. The image force induced by these positive oxide charges, effectively lowering the barrier height on aluminum/oxide interface for Fowler-Nordhein tunneling, heavily degrades the breakdown strength of ECR-SiO_y with an increasing SiH_4/O_2 flow ratio. On the other hand, in a suitable amount, the incorporated F atoms are shown to passivate and neutralize these charged traps, which benefits the breakdown field of F_xSiO_y. However, nonbridge Si-F termination and repulsive force between F and O atoms result in a porous

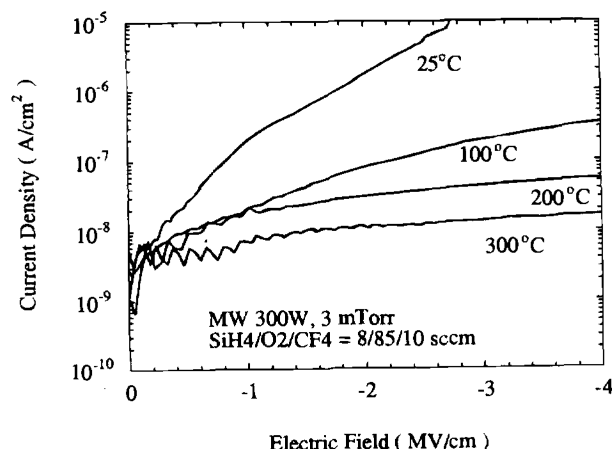

Fig. 11. Variation of F_xSiO_y film pretunneling leakage performance with different deposition temperatures.

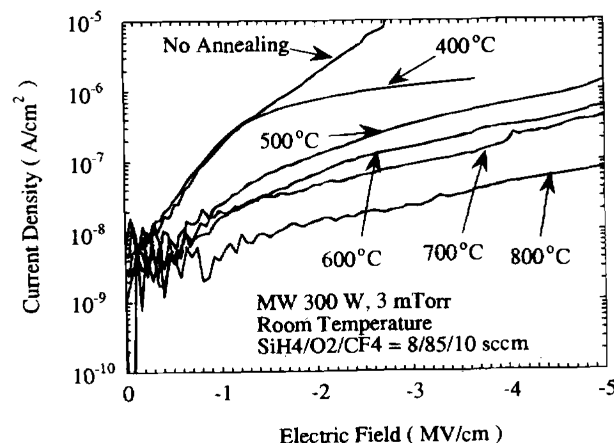

Fig. 13. Variation of pretunneling leakage performance for F_xSiO_y films, deposited at 25°C, before and after annealing at 400, 500, 600, 700, and 800°C (30 min in N_2 ambient).

Downloaded on 2014-04-28 to IP 140.113.38.11 address. Redistribution subject to ECS terms of use (see ecsdl.org/site/terms_use) unless CC License in place (see abstract).

oxide network and hole traps. The excess low-level pre-tunneling leakage current was shown to increase with the incorporated F concentration and even wear out and break down at low field through localized weak spots. Therefore, too much F incorporation in F_xSiO_y raises power consumption and reliability problems. The incorporated F concentration and hence the lowering of the dielectric constant of F_xSiO_y will be limited.

Acknowledgment

This work is supported under Taiwan R.O.C. National Science Council Contract No. NSC 85-2215-E009-061.

Manuscript submitted July 1, 1996; revised manuscript received March 5, 1997.

National Chiao Tung University assisted in meeting the publication costs of this article.

REFERENCES

1. R. K. Laxman, *Semicond. Int.*, **71** (1995).
2. T. Fukada and T. Akahori, in *Proceedings of the First International Dielectrics for VLSI/ULSI Multilevel Interconnection Conference,* p. 43, IEEE, Santa Clara, CA (1995).
3. L. A. Quain, H. W. Fry, G. Nobinger, J. T. Pye, M. C. Schmidt, and J. Cassillas, *ibid.*, p. 50 (1995).
4. S. Takeishi, R. Shinohara, H. Kudoh, A. Tsukune, Y. Satoh, H. Miyazawa, H. Hrada, and M. Yamada, *ibid.*, p. 257 (1995).
5. T. Homma, R. Yamaguchi, and Y. Murao, *This Journal,* **140,** 680 (1993).
6. T. Usami, K. Shimokawa, and M. Yoshimara, *Jpn. J. Appl. Phys.*, **33,** 408 (1994).
7. T. Matsuda, M. J. Shapiro, and S. V. Nguyen, in *Proceedings of the First International Dielectrics for VLSI/ULSI Multilevel Interconnection Conference,* p. 22, IEEE, Santa Clara, CA (1995).
8. K. Musaka, S. Mizuno, and K. Hara, in *International Conference of Solid-State Devices and Materials,* p. 510, Makuhari, Japan (1993).
9. V. L. Shannon and M. Z. Karim, *Thin Solid Films,* **270,** 498 (1995).
10. S. W. Lim, Y. Shimogaki, Y. Nakano, K. Tada, and H. Komiyama, *Appl. Phys. Lett.*, **68,** 832 (1996).
11. S. Takeishi, H. Kudoh, R. Shinohara, A. Tsukune, Y. Satoh, H. Miyazawa, H. Harada, and M. Yamada, *This Journal,* **143,** 381 (1996).
12. K. M. Chang, S. W. Wang, C. J. Wu, T. H. Yeh, C. H. Li, and J. Y. Yang, *Appl. Phys. Lett.*, **69,** 1238 (1996).
13. K. M. Chang, S. W. Wang, C. H. Li, T. H. Yeh, and J. Y. Yang, *ibid.*, Submitted.
14. J. Takahashi, K. Machida, N. Shimoyama, and K. Minegishi, *ibid.*, **62,** 2365 (1993).
15. M. T. Takagi, I. Yoshii, and K. Hashimoto, *Tech. Dig. Electron Devices Meet.*, 703 (1992).
16. N. Shimoyama, K. Machida, J. Takahashi, K. Murase, K. Minegishi, and T. Tsuchiya, *IEEE Trans. Electron. Devices,* **ED-40,** 1682 (1993).
17. K. Machida, N. Shimoyama, J. Takahashi, Y. Takahashi, N. Yabumoto, and E. Arai, *ibid.*, **ED-41,** 709 (1994).
18. E. Kobeda, M. Kellam, and C. M. Osburn, *This Journal,* **138,** 1846 (1991);
19. F. J. Grunthaner, B. F. Lewis, N. Zamini, and J. Maserjian, *IEEE Trans. Nucl. Sci.*, **NS-27,** 1640 (1980).
20. M. Lenzlinger and E. H. Snow, *J. Appl. Phys.*, **40,** 278 (1969).
21. J. Maserjian and N. Zamani, *J. Vac. Sci. Technol.*, **20,** 743 (1982).
22. B. Balland, in *Instabilities in Silicon Devices*, Vol. 1, G. Barbottin and A. Vapaille, Editors, p. 130, North-Holland, Amsterdam (1989).
23. E. Hasegawa, A. Ishitami, K. Akimoto, M. Tsukiji, and N. Ohta, *This Journal,* **142,** 273 (1995).
24. B. Balland and G. Barbottin, in *Instabilities in Silicon Devices,* Vol. 2, G. Barbottin and A. Vapaille, Editors, p. 44, North-Holland, Amsterdam (1989).
25. F. M. Fowkes and D. W. Hess, *Appl. Phys. Lett.*, **22,** 377 (1973).
26. D. J. DiMaria, E. Cartier, and D. Arnold, *J. Appl. Phys.*, **73,** 3367 (1993).
27. A. H. Edwards and W. B. Fowler, *J. Phys. Chem. Solids,* **46,** 841 (1985).
28. A. J. Lelis, H. E. Boesch, Jr., T. R. Oldman, and F. B. Mclean, *IEEE Trans. Nucl. Sci.*, **NS-35,** 1186 (1988).
29. J. K. Rudra and W. B. Fowler, *Phys. Rev. B,* **35,** 8223 (1987).
30. K. L. Yip and W. B. Fowler, *ibid.*, **23,** 2327 (1975).
31. A. J. Bennett and L. M. Roth, *J. Phys. Chem. Solids,* **32,** 1251 (1971).
32. H. Harberland, *Phys. Status Solidi B,* **110,** 521 (1982).
33. H. Mizuno, Y. Ohki, K. Nagasawa, R. Tohmon, Y. Shimpgachi, and Y. Hara, *Phys. Rev. Lett.*, **62,** 1388 (1989).
34. M. K. Mazumber, K. Kobayashi, T. Ogata, J. Mitsuhashi, Y. Mashiko, and H. Koyama, *This Journal,* **143,** 368 (1996).
35. I. C. Chen, S. E. Holland, and C. Hu, *IEEE Trans. Electron Devices,* **ED-32,** 413 (1985).
36. T. H. DiStefano and M. Shatzkes, *J. Vac. Sci. Technol.*, **13,** 50 (1976).
37. M. V. Fischetti, *Phys. Rev.*, **31,** 2099 (1985).
38. T. Nishioka, Y. Ohji, and T. P. Ma, *IEEE Electron. Device Lett.*, **EDL-12,** 134 (1991).
39. P. D. Apte, T. Kubota, and K. C. Saraswat, *This Journal,* **140,** 770 (1993).
40. L. Vishnubhotla, T. Ma, H. Tseng, and P. J. Tobin, *IEEE Electron. Device Lett.*, **EDL-14,** 196 (1993).
41. J. A. Taylor, *J. Vac. Sci. Technol.*, **A9,** 2464 (1991).
42. D. J. Dumin and J. R. Muddux, *IEEE Trans. Electron. Devices,* **ED-40,** 963 (1993).
43. R. Rofan and C. Hu, *IEEE Electron. Device Lett.*, **EDL-12,** 633 (1991).
44. P. Olivo, T. N. Nguyen, and B. Ricco, *IEEE Trans. Electron. Devices,* **ED-35,** 2259 (1988).

Downloaded on 2014-04-28 to IP 140.113.38.11 address. Redistribution subject to ECS terms of use (see ecsdl.org/site/terms_use) unless CC License in place (see abstract).